Communication

Journal of Photopolymer Science and Technology
Volume 32, Number 5 (2019) 715 – 720 ©2019SPST

The Effect of 4-*tert*-Butylpyridine Removal on Efficiency and Thermal Stability in Perovskite Solar Cells

Yongyoon Cho[1,2], Hideo Ohkita[2], Yong Li[1], Jueming Bing[1], Jianghui Zheng[1], Shujuan Huang[1,3], and Anita Ho-baillie[1,3*]

[1] *School of Photovoltaic and Renewable and Engineering, University of New South Wales, Sydney 2052, Australia*
[2] *Department of Polymer Chemistry, Graduate School of Engineering, Kyoto University, Katsura, Nishikyo, Kyoto 615-8510, Japan*
[3] *School of Engineering, Macquarie University, Sydney 2109, Australia*
**a.ho-baillie@unsw.edu.au*

Perovskite solar cells (PSCs) have shown a significant improvement in power conversion efficiency (PCE) in the last few years. However, instability of PSCs is still a barrier for successful industrialization. In particular, spiro-OMeTAD with additives, despite a popular choice for hole transport material (HTM) in PSCs, is one of the causes for device thermal instability. In this work, one of additives in HTM, 4-*tert*-butylpyridine (tBP) is proved to be a factor of device instability under thermal treatment. Simple solution engineering which excludes the use of tBP in the HTM results in better device stability. The origin of thermal stability improvement shown in this work is attributed to the suppression of morphological change of HTM. Further researches towards thermal stability of perovskite material and dopant-free HTM should be essential since tBP removal was not able to solve the thermal stability issue.

Keywords: Perovskite solar cells, Thermal stability, tBP, Additive, Spiro-OMeTAD, HTM

1. Introduction

Perovskite solar cells (PSCs) have generated immense research interests due to their outstanding power conversion efficiency (PCE), which has recently reached 24.2%. The improvement in PCE for PSCs has been the most rapid compared to other types of solar cell technology [1,2]. In addition, ease of bandgap tuning and solution processing enabling low cost production via printing open up new and niche applications such as tandem solar cells, and flexible solar cells provide additional advantages of PSCs [3–5].

However, intrinsic instability of PSCs has been a barrier for their commercialization. Instability under moisture, light, and heat, needs to be addressed for successful deployment in order to make real social contribution for clean energy generation [6–8]. Thermal stability is one of the important parameters as solar cells in the field operate at elevated temperatures [7]. Although by application of composition engineering thermal stability has been improved [9,10], it is still not completely eliminated [11].

Not only does the perovskite layer itself suffers from thermal instability, the hole transport material (HTM) can also be thermally unstable [12–14]. The most popular HTM in PSCs is 2,2′,7,7′-tetrakis[*N*,*N*-di(4-methoxyphenyl)amino]-9,9′-spirobifluorene (spiro-OMeTAD), which typically uses lithium bis(trifluoromethanesulfonyl)imide (Li-TFSI) and 4-*tert*-butylpyridine (tBP) [8,15,16] additives. These additives have been investigated to be harmful for long-term stability of PSCs with ion migration and reaction with perovskite [17]. The tBP has been regarded as a morphology controller of HTM [12–14], but has also been reported to be

Received April 1, 2019
Accepted May 27, 2019

morphology controller in perovskite layer formation that means tBP is able to dissolve perovskite layer [18]. Furthermore, tBP evaporation was reported with morphology change of HTM that caused device instability [12–14].

In this work, PSCs are fabricated without tBP via HTM precursor solvent engineering to find the most desirable composition of chlorobenzene and acetonitrile for best performing tBP-free devices. Thermal test was then conducted afterwards showing advantages of cells without tBP. The reason for this improvement is due to the suppression of HTM morphology deterioration that can be observed in tBP containing device by scanning electron microscope (SEM). However, some levels of thermal degradation still exist in tBP-free devices highlighting the importance of developing dopant-free HTM [19–22].

2. Experimental

2.1. Material preparation

Glass substrates with transparent electrode (fluorine-doped tin-oxide, FTO), formamidium iodide (FAI), methylammonium bromide (MABr) mesoporous TiO_2 paste (m-TiO_2, 30 NR-D) were purchased from Greatcell solar. Lead iodide (PbI_2), lead bromide ($PbBr_2$), dimethylformamide (DMF), dimethyl sulfoxide (DMSO), acetonitrile (ACN), and chlorobenzene (CB) were from Alfa Aesar. Titanium diisopropoxide bis(acetylacetonate), Li TFSI, tBP were gained from Sigma–Aldrich. Spiro-OMeTAD was obtained from Luminescence Technology.

2.2. Precursor solution preparation

To prepare 1.2 M $FAPbI_3$ (or $MAPbBr_3$) solution, the purchased FAI (or MABr) was mixed with PbI_2 (or $PbBr_2$) in DMF:DMSO mixed solvent (4:1 volume ratio) at room temperature. For the solution of $(FAPbI_3)_{0.85}(MAPbBr_3)_{0.15}$, prepared $FAPbI_3$ and $MAPbBr_3$ solutions were mixed with the corresponding volume ratio. In the case of perovskite solution, which we used for this study, extra PbI_2 (5 mol% to $FAPbI_3$) were mixed with the prepared $(FAPbI_3)_{0.85}(MAPbBr_3)_{0.15}$ solution and stirred at room temperature for 30 min.

An HTM solution of containing 72.3 mg spiro-OMeTAD, 17.5 μL of a 520 mg mL^{-1} Li-TFSI in ACN and 31.2 μL of tBP was prepared for the reference device. For tBP-free devices, different solvent mixtures (Table 1) between chlorobenzene and ACN were used to dissolve 72.3 mg spiro-OMeTAD and 17.5 μL of a 520 mg mL^{-1} Li-TFSI in ACN. All solutions were confirmed to be free from Li-TFSI precipitation.

Table 1. Solvent mixture for tBP free devices.

Solvent	Ref.	ACN10	ACN15	ACN20	ACN25
CB	100%	90%	85%	80%	75%
ACN	0%	10%	15%	20%	25%

2.3. Device fabrication

FTO substrates were cleaned with soap water, deionized water, and isopropyl alcohol (IPA) subsequently in ultrasonic bath for 20 min. Then, dense TiO_2 (d-TiO_2) layer was deposited through spray pyrolysis using 180 mM titanium diisopropoxide bis(acetylacetonate) solution that was followed by deposition of m-TiO_2 solution (150 mg mL^{-1} in ethanol) with sintering at 500 °C for 30 min. The prepared perovskite solution was spun at 2000 rpm and 6000 rpm for 20 s and 30 s, respectively, on the prepared substrate. During the last 20 s of the second spin-coating step, the anti-solvent chlorobenzene was dripped for 3 s. The films were dried on a hot plate at 100 °C for 20 min, which results in around 500 nm thickness of the capping perovskite layer on m-TiO_2. Prepared HTM solutions were spin-coated on the perovskite/m-TiO_2/d-TiO_2/FTO substrate at 2000 rpm for 20 s, which resulted in ~200 nm thickness of the HTM layer. All films on m-TiO_2 were prepared in a nitrogen-filled glovebox. A 100 nm gold electrode was afterward deposited by thermal evaporation.

2.4. Characterization

The *J–V* characteristics of the devices were measured on an NREL calibrated Keithley 2400 source meter under 100 mW cm^{-2} (AM 1.5G) simulated sunlight. A black, non-reflective aperture (0.159 cm^2) mask was used over the cells to avoid overestimation of the device current densities associated with the active device area in ambient condition. SEM images were obtained using a field emission SEM (NanoSEM 230).

3. Results and discussion

3.1. Device performance and perovskite morphology

Firstly, we fabricated PSCs to confirm PCE without tBP in HTM. Solubility problem of Li-TFSI salt in HTM solution had been reported if solution does not include tBP [14]. In this work, we changed solution composition of HTM from CB only to mixture of CB and ACN (Table 1). By using mixed solvent, solutions without Li-TFSI precipitation

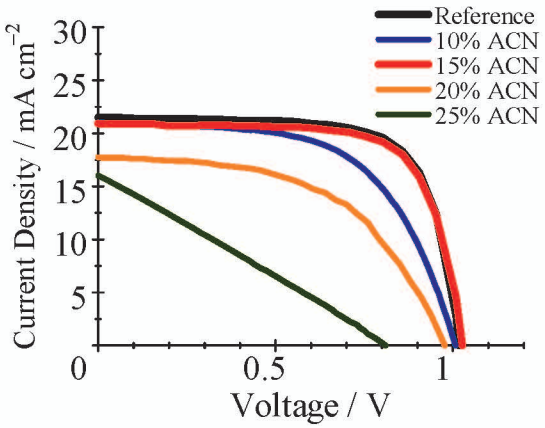

Fig. 1. *J–V* characteristics of perovskite solar cells with (black) and without (red) tBP in the devices. The ACN10, ACN15, ACN20 and ACN25 devices are depicted with blue, red, orange and green lines, respectively.

were obtained.

Figure 1 shows the current–voltage (*J–V*) properties in PSCs of different HTM solutions. In the reference device, an open-circuit voltage (V_{OC}) of 1.017 V, a short-circuit current (J_{SC}) of 21.50 mA cm^{-2}, a fill factor (FF) of 0.7208, and a power conversion efficiency (PCE) of 15.77% were gained. The best PCE amongst the devices without tBP was obtained for the device of 15% ACN mixture solvent (ACN15 in Table 1). The best cell of ACN15 obtained a V_{OC} of 1.029 V, a J_{SC} of 20.89 mA cm^{-2}, an FF of 0.7222, and a PCE of 15.52% that are comparable to those of the reference device. In other composition, however, deteriorated performances were shown.

ACN is known to dissolve perovskite layer [23,24] and incorporation of ACN in HTM solution may impact on perovskite surface by dissolving perovskite resulting in pin holes and/or traps on interface [23]. This is the most possible factor for degraded J-V characteristics in 20% and 25% ACN devices. Thus, we inspected the surfaces of perovskite films after mixed solvent treatment (Figs. 2a-e). Surfaces treated by mixed solvents displayed similar morphologies compared to the reference. However, films with 100% ACN treatment experienced significant change with observable pin holes (Fig. 2f). This result indicates that although perovskites with up to 25% ACN treatment do not show noticeable changes under SEM, point defects caused by the small amount of ACN might have already been formed. In addition, the perovskite/HTM interface might also have been affected resulting in decreasing cell performance as seen by the poorer J-V characteristic as shown in Fig. 1.

Thin film condition varies with solution compositions and process condition [13,25,26]. As ACN concentrations increase, high concentration of Li-salt is likely to segregate easily that the performance of devices drops. Although Li-TFSI is fully dissolved in mixed solvent, spiro-OMeTAD is not in ACN. This can also result in HTM non-uniformity, poor coverage and non-ideal contact with the electrode. The green curve in Fig. 1 shows severe shunting [25,27,28]. J_{SC} drop in 20% and 25% ACN devices is also due to poor carrier collection due to be poor perovskite/HTM interface and defects formation as discussed above.

In conclusion, a mixture of CB (85%) and ACN

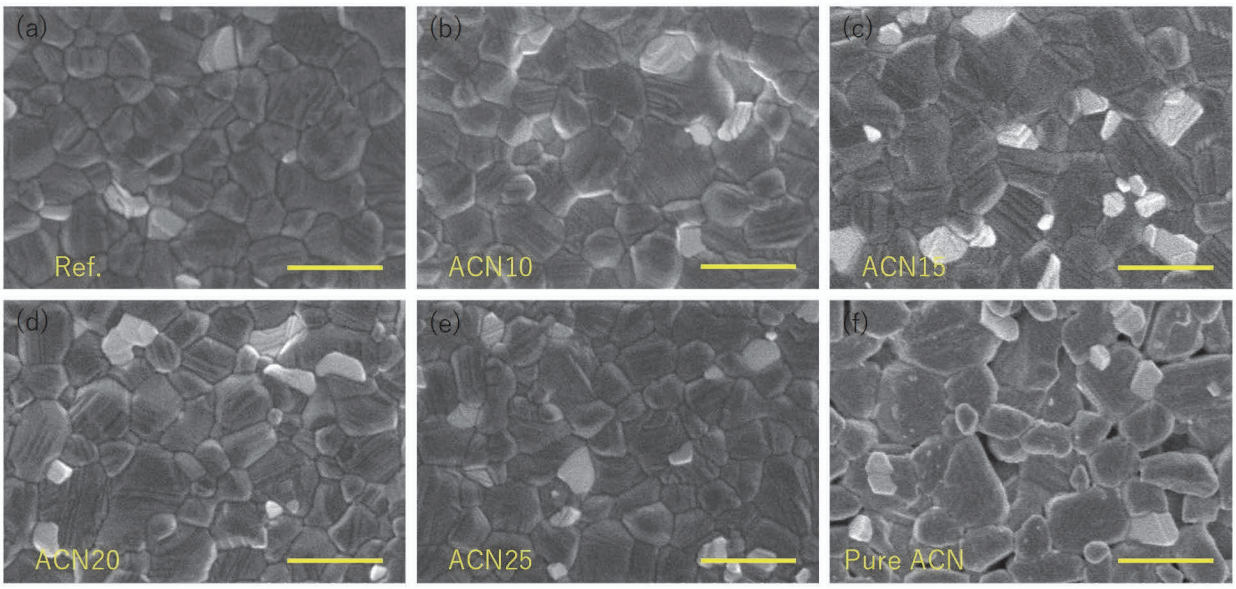

Fig. 2. Perovskite morphologies after mixed-solvent treatment: (a) 0% ACN, (b) 10% ACN, (c) 15% ACN, (d) 20% ACN, (e) 25% CAN, and (f) 100% ACN. Scale bar indicates 500 nm.

(15%) is suitable for the fabrication of tBP-free devices that solves the difficulty of Li-TFSI solubility without adversely affecting perovskite and HTM morphologies. Furthermore, a similar performance was achieved in the ACN15 device and the reference as shown in Fig. 1, the red and black curves, respectively.

3.2. Thermal stability

To investigate the effect of tBP removal on the thermal-stability of ACN15 devices, PCEs of these cells with and without tBP were measured after the thermal test which is a hot plate treatment at 80 °C for 6 hours inside a nitrogen-filled glove box to eliminate the effect of oxygen or humidity.

The *J–V* curves of tBP-containing and tBP-free devices after the thermal treatment are shown in Fig. 3. A V_{OC} of 0.9278 V, a J_{SC} of 19.86 mA cm^{-2}, an FF of 0.6989, and a PCE of 12.88% were obtained for the tBP-free device whilst the tBP-containing device showed a V_{OC} of 0.9295 V, a J_{SC} of 18.51 mA cm^{-2}, an FF of 0.6104, and a PCE of 10.50%. All of parameters in both devices decreased from original values after the thermal test. There is however a difference: the device without tBP (ACN15) exhibits better performance compared to the reference device.

The biggest contributor to PCE drop was the decrease in FF by over 10% in the tBP-containing device while the FF drop was only around 2.5% in the tBP-free cell. Increased parasitic resistance mainly influences FF with charge transport, conductivity and interfacial contact hindrances [23]. The J_{SC} showed a similar tendency to FF that the tBP-free device kept 95% of the original value after the heat treatment. On the contrary, tBP-containing device maintained only 86% of its initial J_{SC}. It is

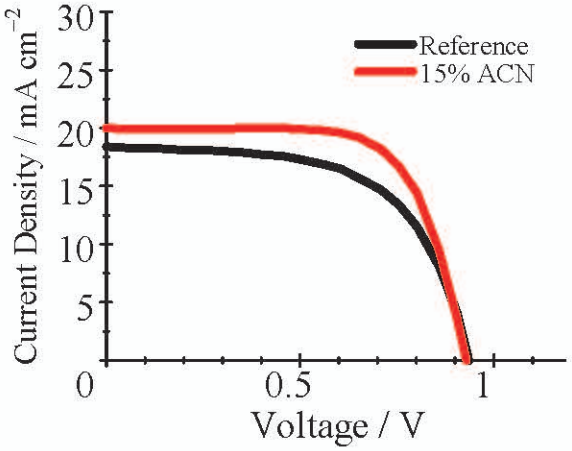

Fig. 3. *J–V* characteristics of perovskite solar cells with (black) and without (red) tBP in the devices after the thermal treatment.

suggested that tBP-induced porous morphology in HTM promoted perovskite degradation [14]. Methylammonium (MA) incorporated perovskite layer is known to be unstable due to its own intrinsic instability [29,30]. The drop in J_{SC} and FF in both devices are expected to be from perovskite instability with morphological change in HTM. Similar decrease of V_{OC} shown in Fig. 3 may not stem from tBP, but from material problem of spiro-OMeTAD itself or perovskite [6,30].

3.3. Change of HTM morphology

In order to examine the stability difference in thermal test, HTM morphology was monitored before and after the thermal treatment. Samples were prepared with device structures except Au electrode evaporation for direct monitoring of HTM change. Figure 4 presents HTM morphologies of the reference device (a,b) and tBP-free device (c,d) before (a,c) and after (b,d) the thermal test. In Figs. 4a and 4c, morphologies of HTM are similar regardless of tBP existence. Interestingly, after the thermal test, the discrepancy becomes apparent: surface of tBP-free HTM unchanged (Fig. 4d) whereas tBP-containing HTM showed changed morphology with appearance of white spots and circular patterns. There are several reports for negative effects of tBP on HTM morphology: voids generation in spiro-OMeTAD [12–14]. These changes in Fig. 4 can be attributed to pores generated in HTM that is consistent with observations in previous study after thermal treatment [12]. Thus, it is indicative that tBP morphology change from the thermal treatment is suppressed in the tBP-free devices.

It is consistent with our device performance result. Through these voids, irreversible degradation reaction can take place under accelerated lifetime test condition such as thermal cycling [11]. Gold migration may be accelerated through these holes that decrease shunt resistance [31]. This morphological change adversely affects interfacial contact and therefore conductivity and charge collection [23]. Therefore, stability difference shown in Fig. 3 between the tBP-containing and tBP-free cells is concluded from the HTM morphology change by tBP existence.

4. Conclusion

PSCs without tBP in the HTM were fabricated through solution engineering exhibiting respectable performance compared to the tBP-containing device. The devices with and without tBP presented

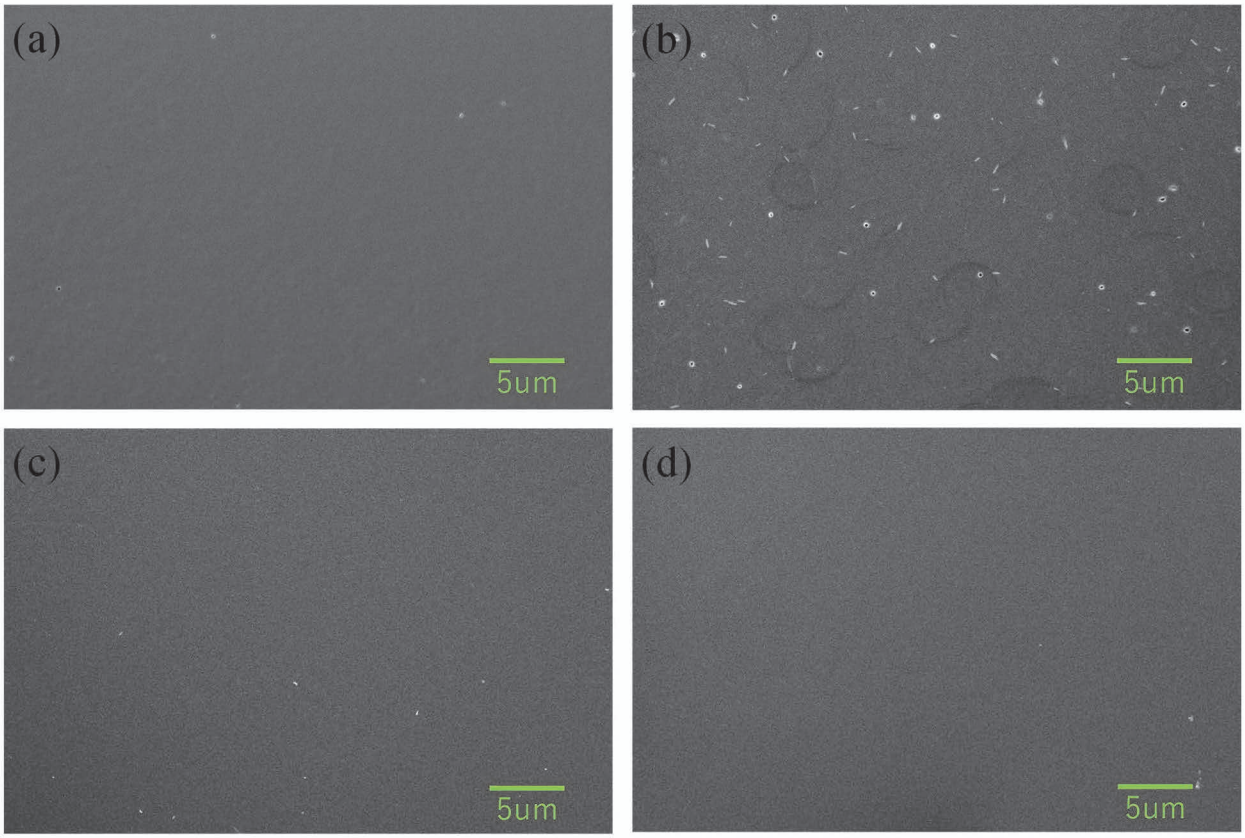

Fig. 4. HTM morphologies in the devices without gold evaporation: before (a) and after (b) the thermal test in the reference, and before (c) and after (d) the thermal test in the device excluding tBP (ACN15).

different results after the thermal treatment. The tBP-free device showed less degradation in PCE, especially in J_{SC} and FF. The SEM result demonstrated that the thermal treatment caused morphology aggravation in the tBP-containing spiro-OMeTAD layer while this deterioration is not observed in the tBP-free layer. The thermal stability was not however totally eliminated yet in the tBP-free devices as V_{OC} decreased regardless of tBP existence. The V_{OC} reduction suggests an increase in trap density, non-radiative recombination and/or a decline of shunt resistance after the thermal treatment. There are still other factors that affect device thermal stability except tBP [6,17,30]. Intrinsic interfacial defects and perovskite instability can be other factors for thermal instability [23], apart from the fact that additive in HTM is harmful. For further improvement of thermal stability in PSCs, further studies for thermal stability of perovskite itself and the development of dopant-free HTM are necessary [21,32].

Acknowledgments

Australian Centre for Advanced Photovoltaics (ACAP) encompasses the Australian-based activities of the Australia U.S. Institute for Advanced Photovoltaics (AUSIAPV) and is supported by the Australian Government through the Australian Renewable Energy Agency (ARENA). The authors thank the researchers and Analytical Centre at UNSW for their support.

References

1. "Efficiency chart", https://www.nrel.gov/pv/cell-efficiency.html.
2. M. A. Green, Y. Hishikawa, E. D. Dunlop, D. H. Levi, J. Hohl-Ebinger, and A. W. Y. Ho-Baillie, *Prog. Photovoltaics Res. Appl.*, **1** (2018) 3.
3. J. Zheng, L. Hu, J. S. Yun, M. Zhang, C. F. J. Lau, J. Bing, X. Deng, Q. Ma, Y. Cho, W.-F. Fu, C. Chen, M.A. Green, S. Huang, and A. W. Y. Ho-Baillie, *ACS Appl. Energy Mater.*, **2** (2018) 561.
4. C. Bi, B. Chen, H. Wei, S. DeLuca, and J. Huang, *Adv. Mater.*, **30** (2017) 1605900.
5. M. Najafi, F. Di Giacomo, D. Zhang, S. Shanmugam, A. Senes, W. Verhees, A. Hadipour, Y. Galagan, T. Aernouts, S. Veenstra, and R. Andriessen, *Small*, **14** (2018) 1702775.
6. A. Dualeh, P. Gao, S. Il Seok, M. K. Nazeeruddin, and M. Grätzel, *Chem. Mater.*, **21** (2014) 6160.

7. K. Domanski, E. A. Alharbi, A. Hagfeldt, M. Grätzel, and W. Tress, *Nat. Energy*, **1** (2018) 61.
8. Y. Cho, A. M. Soufiani, J. S. Yun, J. Kim, D. S. Lee, J. Seidel, X. Deng, M. A. Green, S. Huang, and A. W. Y. Ho-Baillie, *Adv. Energy Mater.*, **20** (2018) 1703392.
9. L.-Q. Xie, L. Chen, Z.-A. Nan, H.-X. Lin, T. Wang, D. Zhan, J.-W. Yan, B.-W. Mao, and Z.-Q. Tian, *J. Am. Chem. Soc.*, **9** (2017) 3320.
10. M. Saliba, T. Matsui, J.-Y. Seo, K. Domanski, J.-P. Correa-Baena, M. K. Nazeeruddin, S. M. Zakeeruddin, W. Tress, A. Abate, A. Hagfeldt, and M. Grätzel, *Energy Environ. Sci.*, **6** (2016) 1989.
11. L. Shi, T. L. Young, J. Kim, Y. Sheng, L. Wang, Y. Chen, Z. Feng, M. J. Keevers, X. Hao, P. J. Verlinden, M. A. Green, and A. W. Y. Ho-Baillie, *ACS Appl. Mater. Interfaces*, **30** (2017) 25073.
12. A. K. Jena, M. Ikegami, and T. Miyasaka, *ACS Energy Lett.*, **8** (2017) 1760.
13. E. J. Juarez-Perez, M. R. Leyden, S. Wang, L. K. Ono, Z. Hawash, and Y. Qi, *Chem. Mater.*, **16** (2016) 5702.
14. S. Wang, M. Sina, P. Parikh, T. Uekert, B. Shahbazian, A. Devaraj, and Y. S. Meng, *Nano Lett.*, **9** (2016) 5594.
15. J. Bing, J. Kim, M. Zhang, J. Zheng, D. S. Lee, Y. Cho, X. Deng, C. F. J. Lau, Y. Li, M. A. Green, S. Huang, and A. W. Y. Ho-Baillie, *Small*, **15** (2019) 1804858.
16. J. Zheng, C. F. J. Lau, H. Mehrvarz, F.-J. Ma, Y. Jiang, X. Deng, A. Soeriyadi, J. Kim, M. Zhang, L. Hu, X. Cui, D.S. Lee, J. Bing, Y. Cho, C. Chen, M. A. Green, S. Huang, and A. W. Y. Ho-Baillie, *Energy Environ. Sci.*, **9** (2018) 2432.
17. Z. Li, C. Xiao, Y. Yang, S.P. Harvey, D. H. Kim, J. A. Christians, M. Yang, P. Schulz, S. U. Nanayakkara, C.-S. Jiang, J. M. Luther, J. J. Berry, M. C. Beard, M. M. Al-Jassim, and K. Zhu, *Energy Environ. Sci.*, **8** (2017) 1234.
18. Y. Shi, X. Wang, H. Zhang, B. Li, H. Lu, T. Ma, and C. Hao, *J. Mater. Chem. A*, **3** (2015) 22191.
19. L. Kegelmann, P. Tockhorn, C. M. Wolff, J. A. Márquez, S. Caicedo-Dávila, L. Korte, T. Unold, W. Lövenich, D. Neher, B. Rech, and S. Albrecht, *ACS Appl. Mater. Interfaces*, **9** (2019) 9172.
20. B. Wang, Q. Zeng, Z. Sun, S. Xue, and M. Liang, *Dye. Pigment*, **165** (2019) 81.
21. H. D. Pham, T. T. Do, J. Kim, C. Charbonneau, S. Manzhos, K. Feron, W. C. Tsoi, J. R. Durrant, S. M. Jain, and P. Sonar, *Adv. Energy Mater.*, **16** (2018) 1703007.
22. H. D. Pham, K. Hayasake, J. Kim, T. T. Do, H. Matsui, S. Manzhos, K. Feron, S. Tokito, T. Watson, W. C. Tsoi, N. Motta, J. R. Durrant, S. M. Jain, and P. Sonar, *J. Mater. Chem. C*, **14** (2018) 3699.
23. H. Tao, Y. Li, C. Zhang, K. Wang, B. Tan, J. Wang, and J. Tao, *J. Phys. Chem. Solids*, **123** (2018) 25.
24. M. T. Klug, N. K. Noel, L. M. Herz, H. J. Snaith, J. Lim, D. P. McMeekin, J. H. Warby, S. Mahesh, M. B. Johnston, and J. M. Ball, *Joule*, **2** (2019) 387.
25. J. Lian, Q. Wang, Y. Yuan, Y. Shao, and J. Huang, *J. Mater. Chem. A*, **5** (2015) 9146.
26. Z. Liu, L. Krückemeier, B. Krogmeier, B. Klingebiel, J. A. Márquez, S. Levcenko, S. Öz, S. Mathur, U. Rau, T. Unold, and T. Kirchartz, *ACS Energy Lett.*, **4** (2019) 110.
27. D. B. Khadka, Y. Shirai, M. Yanagida, and K. Miyano, *J. Mater. Chem. C*, **6** (2018) 162.
28. M. T. Hörantner, P. K. Nayak, S. Mukhopadhyay, K. Wojciechowski, C. Beck, D. McMeekin, B. Kamino, G. E. Eperon, and H. J. Snaith, *Adv. Mater. Interfaces*, **10** (2016) 1500837.
29. D. P. McMeekin, G. Sadoughi, W. Rehman, G. E. Eperon, M. Saliba, M. T. Horantner, A. Haghighirad, N. Sakai, L. Korte, B. Rech, M. B. Johnston, L. M. Herz, and H. J. Snaith, *Science*, **6269** (2016) 151.
30. B. Conings, J. Drijkoningen, N. Gauquelin, A. Babayigit, J. D'Haen, L. D'Olieslaeger, A. Ethirajan, J. Verbeeck, J. Manca, E. Mosconi, F. De Angelis, and H.-G. Boyen, *Adv. Energy Mater.*, **15** (2015) 1500477.
31. S. Cacovich, L. Ciná, F. Matteocci, G. Divitini, P. A. Midgley, A. Di Carlo, and C. Ducati, *Nanoscale*, **14** (2017) 4700.
32. E. H. Jung, N. J. Jeon, E. Y. Park, C. S. Moon, T. J. Shin, T.-Y. Yang, J. H. Noh, and J. Seo, *Nature*, **7749** (2019) 511.